ISSN 0010-5082, Combustion, Explosion, and Shock Waves, 2015, Vol. 51, No. 4, pp. 502–510. © Pleiades Publishing, Ltd., 2015.
Original Russian Text © Z. Zhang, L. Sun, X. Yao, X. Cao.

Smoothed Particle Hydrodynamics Simulation of the Submarine Structure Subjected to a Contact Underwater Explosion

Z. Zhang[a], L. Sun[a], X. Yao[a], and X. Cao[a]

UDC 523.593

Published in *Fizika Goreniya i Vzryva*, Vol. 51, No. 4, pp. 116–125, July–August, 2015.
Original article submitted January 23, 2014; revision submitted November 6, 2014.

Abstract: In this paper, a modified smoothed particle hydrodynamics (SPH) formula is deduced to solve the problem of interfaces with a high density ratio. Simplified SPH models for single and double cylindrical shells (abbreviated as single-hull and double-hull models, respectively) are established to study shock wave propagation and to conduct the damage analysis. The SPH results for the single-hull model are verified by AUTODYN. In addition, the damage analysis indicates that the single-hull model is damaged more severely than the double-hull model. The inner shell in the double-hull model is protected by a water interlayer.

Keywords: damage characteristics, contact underwater explosion, cylindrical shell, SPH method, water interlayer.

DOI: 10.1134/S0010508215040164

INTRODUCTION

An underwater explosion is a subdiscipline of explosive dynamics, involving detonation shock dynamics, mechanics of explosion, etc. Research on underwater explosions by experimental and theoretical methods, as well as numerical simulations, have been carried out by experts and scholars for decades [1–7]. Tests on scaled models were performed to rule out the effect of the submergence depth on the damage potential of the underwater explosion [8, 9]. Experiments on circular high-strength low-alloy (HSLA) steel plates in air were employed to establish the fraction of the explosive energy transferred to the plates [10]. A series of experiments was conducted to summarize the failure mode of a thin sheet [11]. Experiments on a warship structure subjected to an underwater contact explosion were performed to explore the damage characteristics of ship structures [12]. However, experimental research is limited due to high cost and safety issues. Therefore, a theoretical analysis combined with numerical simulations is generally used to study underwater explosions at present. The failure process of a rectangular plate and a circular plate was studied through analytical solutions and numerical solutions [13, 14]. Numerical simulations with the arbitrary Eulerian Lagrangian (ALE) method were employed to investigate the survival capability of a damaged submarine liquefied oxygen tank subjected to an underwater explosion [15]. All these researchers made use of the traditional grid method to deal with nonlinear problems of an underwater explosion. However, computational difficulties may be caused by grid distortion. For this reason, the smoothed particle hydrodynamics (SPH) method with mesh-free properties is applied in this paper, which has an advantage of dealing with large deformations [16]. Numerical simulations with the SPH method were performed to verify its feasibility and superiority to simulate underwater explosions [17–20].

[a] College of Shipbuilding and Ocean Engineering, Harbin Engineering University, 150001 Harbin, China; heuzhangzhifan@gmail.com.

A single cylindrical shell model and a double cylindrical shell model are abbreviated in this paper as a single-hull model and a double-hull model, respectively, in the following contents. First, an SPH model of a free-field underwater explosion is established, and the results are compared with those predicted by an empirical formula to verify the validity and feasibility of the SPH method. Second, shock wave propagation in multilayer materials is investigated. The result of shock wave propagation of the single-hull model is compared with that computed by the AUTODYN commercial software, and the results of this comparison verified the robustness and high accuracy of the SPH method in solving nonlinear problems. Third, the damage analysis of the single-hull and the double-hull models is conducted, including the failure mode analysis, elastoplastic partition, crevasse, and deflection analysis. In addition, the influence of different amounts of interlayer water on explosion prevention is discussed.

1. THEORETICAL BACKGROUND

1.1. SPH Formulation at High Density Ratios

A harmonious combination of the particle property with the Lagrange nature makes the SPH method suitable for simulating interfaces in different materials. The accuracy with the standard SPH formula can be guaranteed if the materials have similar densities (if the density ratio is low). However, with an increase in the density ratio, the accuracy cannot be guaranteed by the standard SPH method; in this case, the SPH method should be modified.

The modified SPH approximate formula has advantages of handling high density ratios. Let particles i and j be a pair of interacting particles. The approximate function formula [21] for the ith particle is

$$\Gamma(\boldsymbol{x}_i) = \sum_{j=1}^{N} \frac{m_j}{\rho_j} \Gamma(\boldsymbol{x}_j) W_{ij}, \tag{1}$$

where m is the particle mass, ρ is the density, and W_{ij} is the piecewise-linear smoothing cubic spline [21]. According to the equal volumes V of adjacent particles and the approximate function formula, the density can be written as

$$\rho_i = \frac{1}{V_i} \sum_{j=1}^{N} m_i V_j W_{ij}$$

$$= \sum_{j=1}^{N} m_i \frac{V_j}{V_i} W_{ij} = \sum_{j=1}^{N} m_i W_{ij}. \tag{2}$$

The mass conservation law takes the form [21]

$$\frac{d\rho_i}{dt} = -\rho_i \sum_{j=1}^{N} \frac{m_j}{\rho_j} \boldsymbol{v}_j^b \frac{\partial W_{ij}}{\partial \boldsymbol{x}_i^b} = -m_i \sum_{j=1}^{N} \boldsymbol{v}_j^b \frac{\partial W_{ij}}{\partial \boldsymbol{x}_i^b}, \tag{3}$$

where $\boldsymbol{v}$ is the velocity of particles, $\boldsymbol{x}$ is the displacement of particles, and a and b indicate two different coordinate directions. Assuming that $\Gamma(x_i)$ in Eq. (1), we obtain

$$\frac{m_i}{\rho_i} \sum_{j=1}^{N} \frac{\partial W_{ij}}{\partial \boldsymbol{x}_i^b} = \sum_{j=1}^{N} \frac{m_i}{\rho_i} \frac{\partial W_{ij}}{\partial \boldsymbol{x}_i^b} = \text{grad}1 = 0. \tag{4}$$

Both sides of Eq. (4) shall be multiplied by $\rho_i \boldsymbol{v}_i^b$, which yields

$$m_i \sum_{j=1}^{N} \boldsymbol{v}_j^b \frac{\partial W_{ij}}{\partial \boldsymbol{x}_i^b} = m_i \boldsymbol{v}_j^b \sum_{j=1}^{N} \frac{\partial W_{ij}}{\partial \boldsymbol{x}_i^b} = 0. \tag{5}$$

In view of Eqs. (3) and (5), the continuity equation can be written as

$$\frac{d\rho_i}{dt} = m_i \sum_{j=1}^{N} \boldsymbol{v}_{ij}^b \frac{\partial W_{ij}}{\partial \boldsymbol{x}_i^b}. \tag{6}$$

As it follows from [21], the discrete form of the momentum conservation equation and the energy conservation equation can be written as

$$\frac{d\boldsymbol{v}_i^a}{dt} = -\sum_{j=1}^{N} \frac{m_j}{\rho_j} \left(\frac{p_i + p_j}{\rho_i} + \Pi_{ij} \right) \frac{\partial W_{ij}}{\partial \boldsymbol{x}_i^a}$$

$$+ \sum_{j=1}^{N} \frac{m_j}{\rho_j} \frac{S_i^{ab} + S_j^{ab}}{\rho_i} \frac{\partial W_{ij}}{\partial \boldsymbol{x}_i^b}, \tag{7}$$

$$\frac{de_i}{dt} = \frac{1}{2} \sum_{j=1}^{N} \frac{m_j}{\rho_j} \left(\frac{p_i + p_j}{\rho_i} + \Pi_{ij} \right) \boldsymbol{v}_{ij}^b \frac{\partial W_{ij}}{\partial \boldsymbol{x}_i^b} + \frac{1}{\rho_i} S_i^{ab} \varepsilon_i^{ab}. \tag{8}$$

Here p is the pressure, e is the internal energy, t is the time, ε is the displacement of particles, and S is the viscous shear stress.

1.2. Constitutive Equation

For solids, the stress σ is composed of the isotropic pressure p and the deviatoric stress tensor S; for fluids, it is composed of the isotropic pressure p and the viscous shear stress τ [21]:

$$\sigma^{ab} = -p\delta^{ab} + S^{ab}, \tag{9}$$

$$\sigma^{ab} = -p\delta^{ab} + \tau^{ab} \tag{10}$$

(δ^{ab} is the Kronecker delta). For detonation products, the pressure p can be obtained from the Jones–Wilkins–Lee (JWL) equation of state [22]; for water, it can be found from the Mie–Grüneisen equation of state [23];

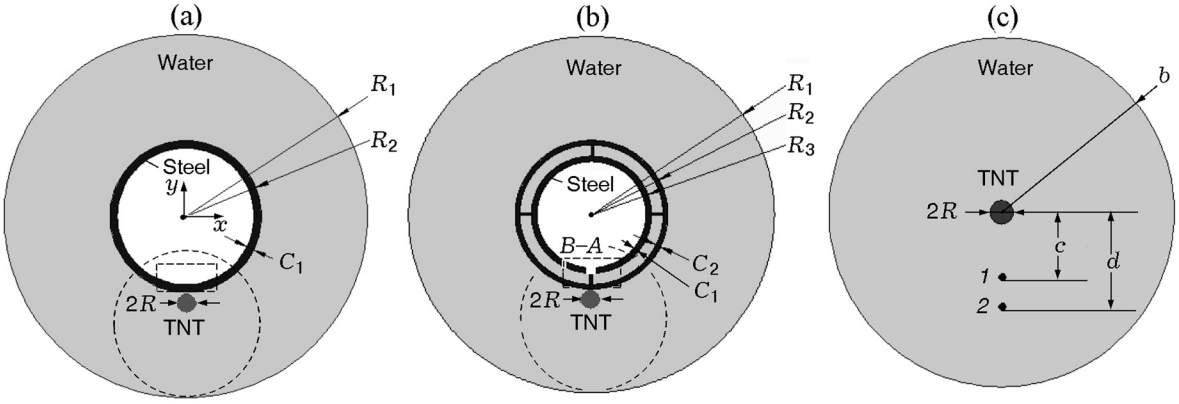

Fig. 1. Single-hull (a), double-hull (b), and free-field (c) underwater explosions in water: the circular and rectangular regions are domains in which the pressure and equivalent plastic strain were calculated, respectively; the test points are indicated by *1* and *2*.

Parameters of the shell models

Model	Water		Outside radius, m		Shell thickness, m		TNT charge radius, m
	outside radius, m	inside radius, m	inner shell	outer shell	inner shell	outer shell	
Single-hull model	7.5	3.528	3.528	—	0.028	—	0.1
Double-hull model	7.5	4.318	3.528	4.318	0.028	0.018	0.1

finally, for steel, the value of p can be obtained from the solid Mie–Grüneisen equation of state [24].

For solids, the deviatoric stress S can be calculated from the deviatoric stress rate $\dot{S}$, given by the Jaumann stress rate [21]. The Johnson–Cook [25] model is used to calculate the yield strength. The von Mises yield criterion is used to determine whether the stress should be renewed through a comparison between the Mises stress and the yield strength; in this case, the deviatoric stress S should be modified as in [26]:

$$S^{ab} = S^{ab}\frac{Y}{\sigma_{\text{Mises}}} \tag{11}$$

(Y is the yield strength).

1.3. Reflection and Transmission of the Shock Wave

The shock wave propagates from material 1 to material 2. The variables such as the density ρ, pressure p, particle velocity u, and shock wave velocity D change after shock wave propagation. Let us denote these variables ahead of and behind the shock wave by the subscripts 1 and 2 ($\rho_1 D_1$ and $\rho_2 D_2$ are the impedances of materials 1 and 2, respectively). According to the impedance matching principle, shock wave propagation in various materials can be divided into two cases [27]: the reflected wave is a compression wave at $\rho_1 D_1 < \rho_2 D_2$ and a rarefaction wave at $\rho_1 D_1 > \rho_2 D_2$. Taking the single-hull model as an example, we can see that a transmitted wave propagates in steel after the shock wave propagates from water to steel, while a compression wave is reflected into water.

2. CYLINDRICAL SHELL SUBJECTED TO A CONTACT UNDERWATER EXPLOSION

2.1. Models and Parameters

The outer shell is in direct contact with a torpedo when the submarine structure is attacked. The torpedo is modeled by a TNT charge. All models are considered in the same coordinate system with the origin being located at the center of the water domain. The structures of the single-hull submarine and the double-hull submarine are simplified and considered as cylindrical steel shells (Fig. 1). The domains in which the pressure and the equivalent plastic strain were calculated are marked out by the circular region and the rectangular region in Fig. 1, respectively.

Considering the number of particles, we choose one half of the entire model as a research object. A uniform distribution of particles is adopted, and the distance between the particles is set to $5 \cdot 10^{-3}$ m. Therefore, there

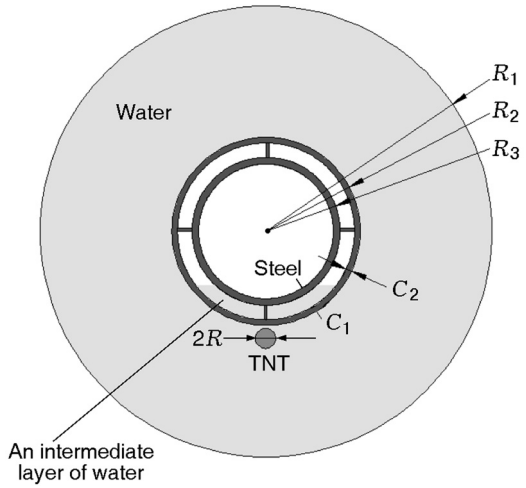

Fig. 2. Double-hull model with an interlayer filled by water (25%).

are 689 119 particles for the single-hull model, 603 247 particles for the double-hull model with no water interlayer, and 698 725 particles for the double-hull model with a completely filled water interlayer. To find the influence of the water interlayer, the double-hull model is simulated with the intermediate layer filled by water at 100, 75, 50, and 25% of its capacity (Fig. 2), as well as the case with no water interlayer. Figure 1 shows the test points A (0, −3.527) and B (−3.285, −3.504); the model parameters are summarized in the table.

2.2. Numerical Model

The numerical model for verification of the effectiveness of the SPH method is shown in Fig. 1c. It has the following parameters: the TNT charge radius is R =0.1 m, the radius of the water domain is b =0.3 m, the distance from the explosion center to the test point *1* is $c = 1.5$ m, the distance from the explosion center to the test point *2* is $d = 2.0$ m, and the spacing between the water and steel particles is $dx = 0.01$ m. The explosion center is located at the center of the TNT charge, which has a weight of 51.2 kg.

The analytical formula developed by Zamyshlyayev [28] and AUTODYN computations are used to verify the results calculated by the SPH method. The difference between these results (Fig. 3) does not exceed 10%. Disturbances observed in the numerical results are probably induced by numerical errors. Moreover, the pressure predicted by the empirical formula [28] decreases slightly faster than the numerical results, and it may be caused by the fluid viscosity and numerical errors. Thus, the validity and feasibility of the SPH method are verified.

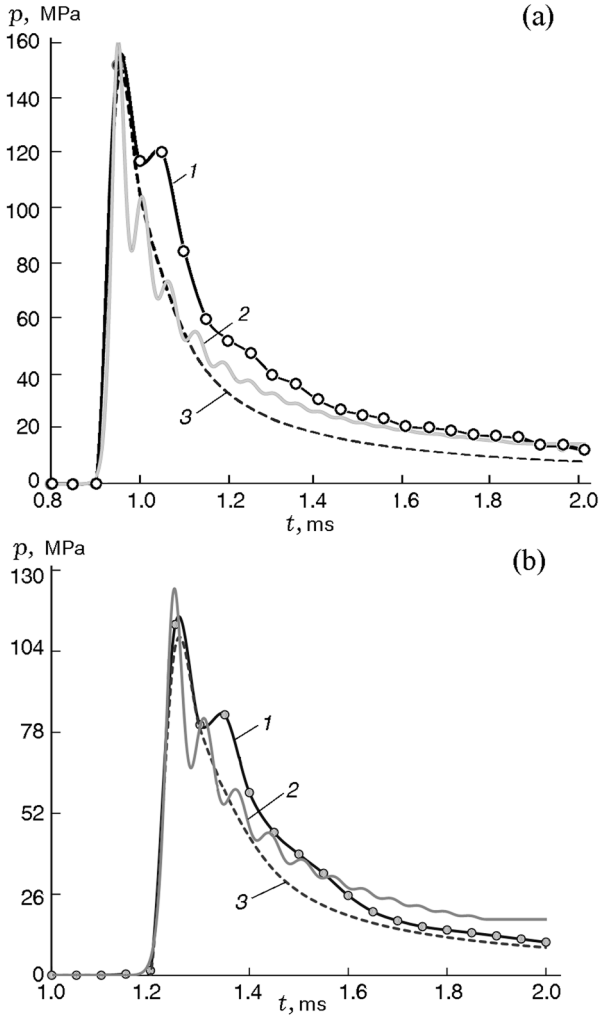

Fig. 3. Pressure curves at the test points *1* (a) and *2* (b): curves *1* and *2* show the results predicted by the SPH method and AUTODYN, respectively; the dashed curves are calculated by the analytical expression from [28].

2.3. Shock Wave Propagation

Case of a Single Cylindrical Shell. The pressure field in the examined area of the shock wave is depicted in Fig. 4. The pressure peak value of several gigapascals is instantaneously reached when the explosion occurs. Meanwhile, a reflected wave and a transmitted wave are generated. The pressure value in the normal direction is higher than in other directions. The reason for this phenomenon is probably that the surge impedance of the explosive is higher than that of steel. As a result, there is not only a transmitted wave generated in steel, but also a compression wave is induced in the explosive. Meanwhile, the compression wave generates the second shock wave in water. Figure 4 also shows that the wave

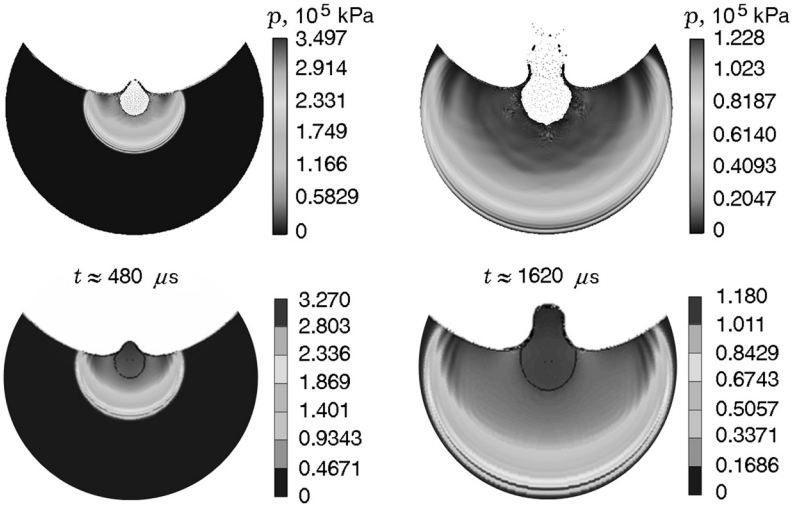

Fig. 4. Pressure field in the single-hull model (circular region in Fig. 1) at different time instants calculated by the SPH method (top) and AUTODYN (bottom).

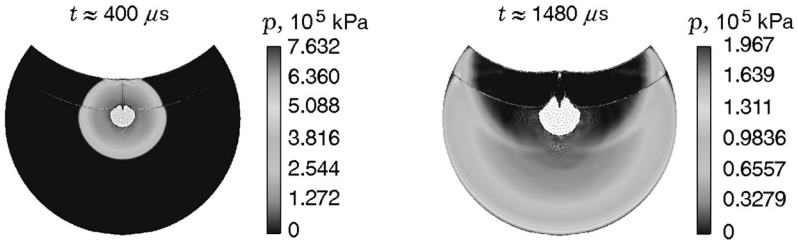

Fig. 5. Pressure field (circular region in Fig. 1) in the double-hull model with the interlayer completely filled by water at different time instants.

propagation velocity in steel is larger than that in water ($t \approx 480$ μs). As a whole, the SPH simulation results are close to the AUTODYN computations.

Case of a Double Cylindrical Shell. The pressure field of the double-hull model containing a water interlayer is shown as Fig. 5. The pressure instantaneously reaches a peak of about several gigapascals when the explosion occurs. Afterwards, the shock wave is repeatedly reflected between the lower surface of the inner shell and the upper surface of the outer shell. At $t \approx 400$ μs, the shock wave arrives at the lower surface of the inner shell, which produces a compression wave in the water interlayer. At the instant $t \approx 1480$ μs, the parameters in this region are caused by the superposition of multiple compression and rarefaction waves, which results in shock load inhomogeneity.

2.4. Damage Analysis

Failure Mode Analysis. As shown in Fig. 6a, the single-hull model deforms seriously at $t \approx 160$ μs, which makes the shell thinner and more fragile. As the shell becomes increasingly thinner due to severe plastic deformation, a crack occurs. The crack expands gradually, and the shell is eventually warped and scattered at $t \approx 1620$ μs. The result shows that the single-hull structure is mainly damaged by the detonation wave and detonation products, and the shell damage mode is consistent with that of a steel plate subjected to an underwater contact explosion [10, 11]. In addition, the failure mode of the outer shell in the double-hull model is similar to that in the single-hull model, passing through several stages illustrated in Fig. 6.

The analysis of the inner shell of the double-hull model is performed for two conditions: with and without the water interlayer. If there is no water interlayer (Fig. 6b), the inner shell is damaged by a large number of high-speed fragments of the damaged outer shell. On the contrary, if the water interlayer is present (Fig. 6c), the inner shell is protected by the water interlayer, which decreases the damage caused by the high-speed fragments.

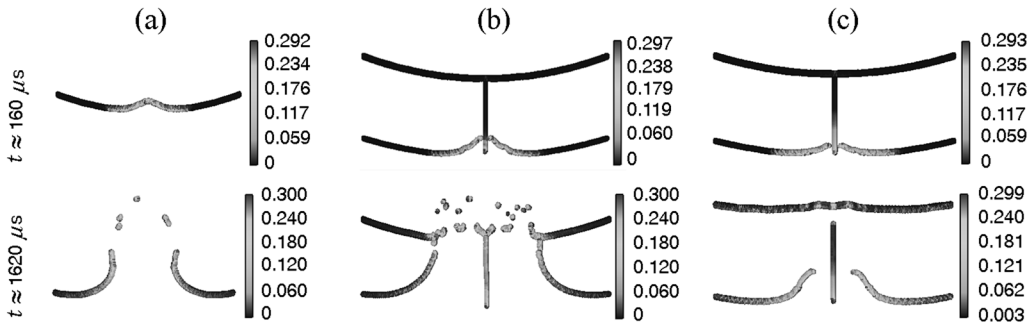

Fig. 6. Equivalent plastic strain (rectangular domain in Fig. 1) at different time instants: (a) single-hull model; (b) double-hull model with no water interlayer; (c) double-hull model filled by water.

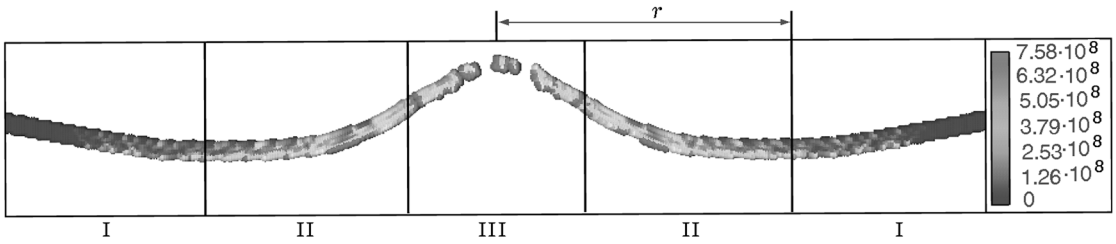

Fig. 7. Elastic–plastic partitioning of the shell.

Elastic–Plastic Partitioning. A thin shell subjected to a contact explosion can be divided into three regions: $0 \leqslant p_{\mathrm{H}} \leqslant \sigma_A$, where the stress and strain are linear functions of pressure, $0 \leqslant p_{\mathrm{H}} \leqslant \sigma_B$, which is the region of plastic deformation, and $p_{\mathrm{H}} \geqslant \sigma_B$, where a solid can be regarded as an isotropic elastic–plastic fluid [29]. Here p_{H} is the detonation pressure, σ_A is the elastic limit of the material, σ_B is the ultimate strength of the material, σ_A =355 MPa, and σ_B = 600 MPa.

As is shown in Fig. 7, the shell can be divided into three sections: elastic region (section I, far from the section that is directly affected by the contact explosion), plastic region (section II, which is closer to the section that is directly affected by the contact explosion and is partially affected by the explosion), and isotropic elastic–plastic region [30] (section III, which is directly in contact with the section subjected to the contact explosion).

Let us introduce a dimensionless variable $H = r/R$, where R is the TNT charge radius and r is the radius of the plastic deformation area in Fig. 7. At $(x/R) \geqslant H$, the influence of plastic deformation can be ignored.

Figure 8 shows the diagram of H. The greater the value of this variable, the greater the plastic deformation region due to a greater level of filling of the double cylindrical shell by water. The reason is probably that a large number of high-speed fragments destroy and scatter the inner shell. In addition, we can find that the radius of the plastic deformation region is very small compared to the overall size of the structure. It means that the structure is only partially damaged owing to the inhomogeneity of the shock load in space. The plastic deformation region for the single-hull model is between the corresponding values for the double-hull structure with the interlayer completely filled by water and the double-hull structure without the water interlayer.

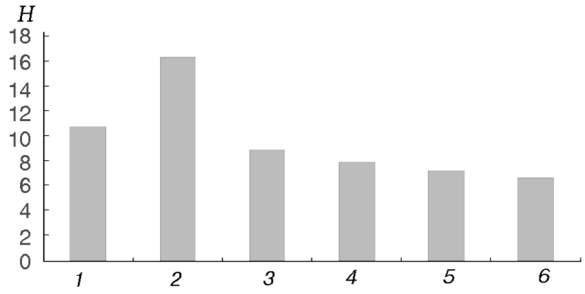

Fig. 8. Diagram of the dimensionless deflection: single-hull model (*1*), double-hull model with the intermediate layer filled by water by 100% (*2*), 75% (*3*), 50% (*4*), and 25% (*5*), and double-hull model with no water interlayer (*6*).

Crevasse and Deflection Analysis. The crevasse curves of the shell (K) for the single hull model and the inner shell of the double-hull model are shown in Fig. 9. The crevasse is normalized by the TNT charge radius.

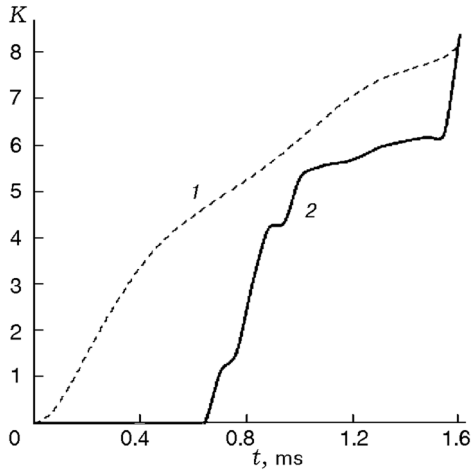

Fig. 9. Crevasse curves for the inner shell versus time: single-hull model (*1*) and double-hull model with no water interlayer (*2*).

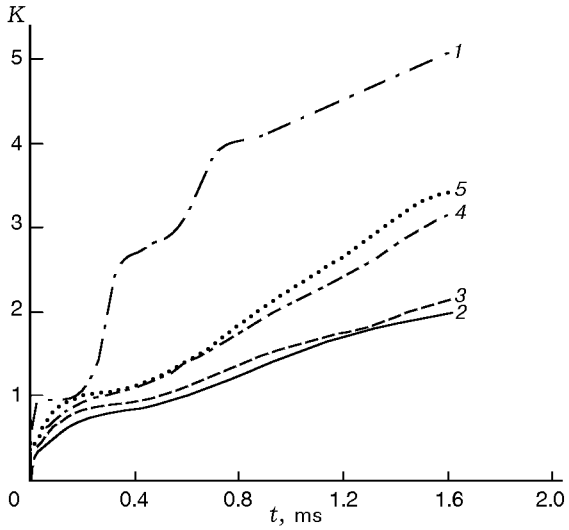

Fig. 10. Crevasse curves for the outer shell versus time for different amounts of water in the interlayer: no water (*1*), 100% of water (*2*), 75% of water (*3*), 50% of water (*4*), and 25% of water (*5*).

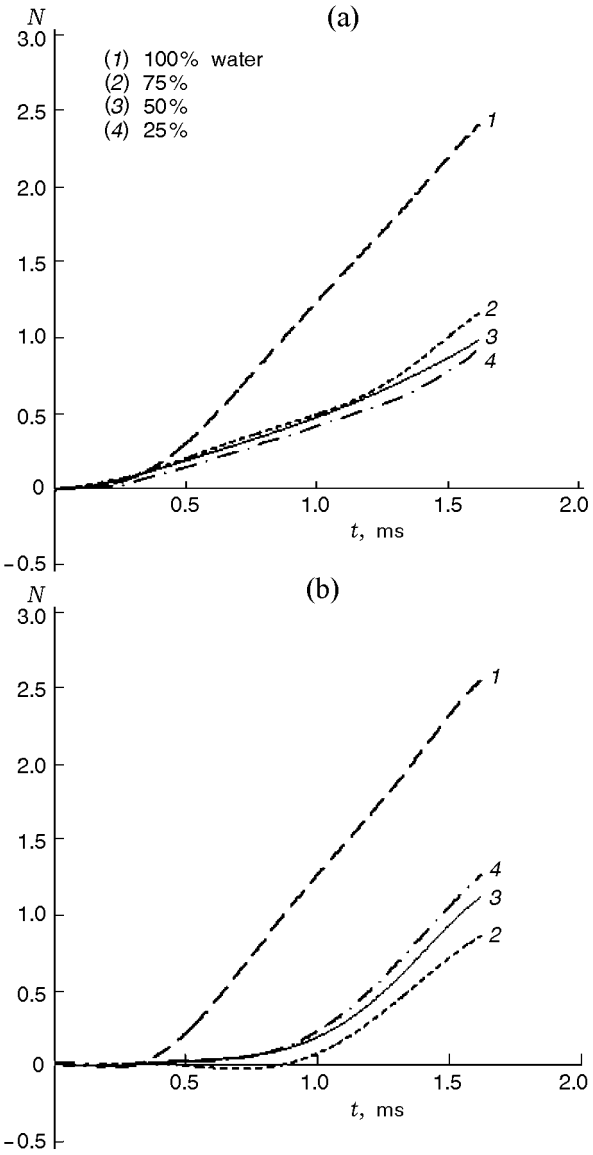

Fig. 11. Deflection curves for the inner shell versus time for different amounts of water in the interlayer at the test points A (a) and B (b).

At $t \approx 1.6$ ms, the crevasse is about eight times greater than the TNT charge radius. The crevasse growth rate for the double-hull model is greater than that of the single-hull model, and there are several salient points on the curves of the double-hull model. Therefore, different failure modes are proved: the single-hull structure is mainly damaged by the detonation wave and detonation products, while the inner shell of the double-hull structure is mainly damaged by a large number of high-speed fragments.

The crevasse curves for the outer shell of the double-hull structure containing different amounts of water in the interlayer are shown in Fig. 10. The greater the amount of interlayer water, the smaller the value of K. In other words, the water interlayer has a certain protective effect on the outer shell. As numerical simulations show, at $t < 1.6$ ms, the crevasse of the inner shell does not occur, and the inner shell merely undergoes plastic deformation.

The influence of the water interlayer on the deflection N is illustrated in Fig. 11 (at the central test point A and the lateral test point B). The deflection is normalized by the TNT charge radius. As is seen in Fig. 11,

at $t \approx 1.6$ ms, the maximum values of the deflection are reached in the case with the interlayer completely filled by water: $N = 2.5$ at point A and $N = 2.0$ at point B. At point A, the deflection becomes larger with increasing water interlayer. At point B, the deflection has the minimum value in the case with the interlayer filled by water by 75%.

CONCLUSIONS

1. The pressure inhomogeneity is caused by the superposition of multiple waves, which further leads to the shock response inhomogeneity.

2. For the single-hull structure, the shell is mainly damaged by the detonation wave and detonation products. For the double-hull structure with no water interlayer, the inner shell is scattered by a large number of high-speed fragments after the outer shell is damaged. The presence of a water interlayer in the double-hull structure reduces the damage caused by the fragments.

3. The submarine structure subjected to a contact explosion can be divided into three regions according to the pressure and strain rate, and the radius of the plastic deformation region can be obtained in each case. The results indicate that the greater the water interlayer, the greater the plastic deformation region, and the shock load is inhomogeneous in space.

4. Through the analysis of crevasses of both the single-hull and double-hull models, we can conclude that the single-hull structure is damaged more seriously than the double-hull structure. The analysis of the crevasse curves proves the fact that the single-hull and double-hull structures have different failure modes.

This work is supported by the Excellent Young Scientists Fund (Grant No. 51222904) and by the National Security Major Basic Research Program of China (Grant No. 613157). Besides, grateful acknowledgement is made to Prof. Zhang Aman and senior fellow apprentice Ming Furen for their considerable help by means of suggestions, comments, and criticism of this work.

REFERENCES

1. A. M. Zhang, L. Y. Zeng, X. D. Cheng, et al., "The Evaluation Method of Total Damage to Ship in Underwater Explosion," Appl. Ocean Res. **33** (4), 240–251 (2011).
2. V. S. Deshpande and N. A. Fleck, "One-Dimensional Response of Sandwich Plates to Underwater Shock Loading," J. Mech. Phys. Solids **53** (11), 2347–2383 (2005).
3. Y. Wang, W. Zhang, H. X. Hua, et al., "Dynamic Response of a Submarine Foam Sandwich Structure Subjected to under Water Explosion." J. Vibr. Shock **29** (4), 64–68 (2010) [in Chinese].
4. A. M. Zhang, W. X. Zhou, S. P. Wang, et al., "Dynamic Response of the Non-Contact Underwater Explosion on Naval Equipment," Marine Struct. **24** (4), 396–411 (2011).
5. U. M. Hans, "Review: Hydrocodes for Structure Response to Underwater Explosion," Shock Vibr. **6** (2), 81–96 (1999).
6. J. W. Swegle and S. W. Attaway, "On the Feasibility of Using Smoothed Particle Hydrodynamics for Underwater Explosion Calculations," Comput. Mech. **17** (3), 151–168 (1995).
7. A. M. Zhang, S. P. Wang, C. Huang, et al., "Influences of Initial and Boundary Conditions on Underwater Explosion Bubble Dynamics," Eur. J. Mech., B: Fluid **42**, 69–91 (2013).
8. A. H. Keil, *Introduction to Underwater Explosion Research* (UERD, Norfolk Naval Ship Yard, Portsmouth, 1956).
9. A. H. Keil, "The Response of Ships to Underwater Explosions," Trans. Soc. Naval Arch. Marine Eng. **69**, 366–410 (1961).
10. R. Rajendran and K. Narasimhan, "Damage Prediction of Clamped Circular Plates Subjected to Contact Underwater Explosion," Int. J. Impact Eng. **25** (4), 373–386 (2001).
11. G. N. Nurick and A. M. Radford, "Deformation and Tearing of Clamped Circular Plates Subjected to Localized Central Blast Loads," in *Recent Developments in Computational and Applied Mechanics: A Volume in Honour of John B. Martin* (International Centre for Numerical Methods in Engineering (CIMNE) (Barcelona, Spain, 1997).
12. R. Q. Liu, X. F. Bai, and X. Zhu, "Breach Experiment Research of Vessel Element Structure Models Subjected to Underwater Contact Explosion," J. Naval Univ. Eng. **13** (5), 41–46 (2001) [in Chinese].
13. Y. W. Lee and T. Wierzbicki, "Fracture Prediction of Thin Plates under Localized Impulsive Loading. Part I: Dishing," Int. J. Impact Eng. **31** (10), 1253–1276 (2005).
14. Y. W. Lee and T. Wierzbicki, "Fracture Prediction of Thin Plates under Localized Impulsive Loading. Part II: Discing and Petaling," Int. J. Impact Eng. **31** (10), 1277–1308 (2005).
15. J. H. Kim and H. C. Shin, "Application of the ALE Technique for Underwater Explosion Analysis of a Submarine Liquefied Oxygen Tank," Ocean Eng. **35** (8/9), 812–822 (2008).
16. M. B. Liu, G. R. Liu, Z. Zong, and K. Y. Lam, "Computer Simulation of High Explosive Explosion using Smoothed Particle Hydrodynamics Methodology," Comput. Fluids **32** (3), 305–322 (2003).
17. A. M. Zhang, W. S. Yang, and X. L. Yao, "Numerical Simulation of Underwater Contact Explosion," Appl. Ocean Res. **34**, 10–20 (2012).

18. A. M. Zhang, W. S. Yang, C. Huang, and F. R. Ming, "Numerical Simulation of Column Charge Underwater Explosion Based on SPH and BEM Combination," Comput. Fluids **1**, 169–178 (2013).
19. A. M. Zhang, F. R. Ming, and S. P. Wang, "Coupled SPHS-BEM Method for Transient Fluid-Structure Interaction and Applications in Underwater Impacts," Appl. Ocean Res. **43**, 223–233 (2013).
20. F. R. Ming, A. M. Zhang, W. S. Yang, et al., "SPH Algorithm to Deal with the Problem of Underwater Contact Explosion of Warship," J. Vibr. Shock **31** (10), 147–151 (2011) [in Chinese].
21. G. R. Liu and M. B. Liu, *Smoothed Particle Hydrodynamics—A Meshfree Particle Method* (World Sci., Singapore, 2003).
22. B. M. Dobratz, *LLNL Explosives Handbook: Properties of Chemical Explosives and Explosives and Explosive Simulants* (Lawrence Livermore Nat. Lab., Livermore, 1981); http://www.osti.gov/scitech/biblio/6530310.
23. D. J. Steinberg, *Spherical Explosions and the Equation of State of Water* (Lawrence Livermore Nat. Lab., Livermore, 1987); http://www.osti.gov/scitech/biblio/6766676.
24. L. D. Libersky, A. G. Petscheck, T. C. Carney, et al., "High Strain Lagrangian Hydrodynamics a Three-Dimensional SPH Code for Dynamic Material Response," J. Comput. Phys. **109** (1), 67–75 (1993).
25. G. R. Johnson and W. H. Cook, "A Constitutive Model and Data for Metals Subjected to Large Strains, High Strain Rates and High Temperatures," in *Proc. 7th Int. Symp. on Ballistics, USA, 1983*.
26. R. V. Mises, "Mechanik der Festen Körper im Plastisch Deformablen Zustand," in *Nachrichten von der Gesellschaft der Wissenschaften zu Göttingen* (Math.-Phys. Klasse, 1913), pp. 582–592.
27. S. Z. Zhang, *Explosion and Shock Dynamics* (Weapon Industry Press, Beijing, China, 1993) [in Chinese].
28. B. V. Zamyshlyayev, *Dynamic Loads in Underwater Explosion* (Naval Intelligince Support Center, Washington, 1973). AD-757183.
29. G. T. Yang, *Introduction to Elasticity and Plasticity* (Tsinghua Univ. Press, Beijing, China, 2004) [in Chinese].
30. J. B. Gai, S. Wang, and P. Tang, "Damage of Thin Plate Subjected to Contact Explosion Loading," J. Harbin Eng. Univ. **27** (4), 523–525 (2006) [in Chinese].